CHEMISTRY OF MATERIALS

pubs.acs.org/cm

Article

Thermogelling Hydroxypropyl Methylcellulose Nanoemulsions as Templates to Formulate Poorly Water-Soluble Drugs into Oral Thin Films Containing Drug Nanoparticles

Liang-Hsun Chen and Patrick S. Doyle*

Cite This: https://doi.org/10.1021/acs.chemmater.2c00801

Read Online

ACCESS | Metrics & More | Article Recommendations | Supporting Information

ABSTRACT: Oral thin films are an emerging solid dosage form for the delivery of poorly water-soluble drugs. Typical thin film formulations require nanomilling of drugs to improve their poor water solubility, followed by incorporating the drug nanoparticles in a polymer solution for casting. However, these formulations are not only inefficient and multistep but also limited to moderate drug loading capacity and susceptible to irreversible nanoparticle aggregation. Based on a widely used film-forming polymer, hydroxypropyl methylcellulose (HPMC), we developed thermogelling nanoemulsions with drug-loaded oil nanodroplets dispersed in a HPMC-loaded water phase. The nanoemulsions can directly act as film precursors for casting and provide robust templates to formulate oral films with uniform drug nanoparticles embedded in a dried HPMC matrix. The thermally gelled network effectively immobilizes the oil nanodroplets for confined nanoparticle crystallization and avoids potential irreversible nanoparticle aggregation, which enables high drug loading contents up to 63 wt %. The oral films also possess a tunable immediate release because the films have large surface-to-volume ratios and the drug nanoparticles are fast-dissolving. Overall, the thermogelling nanoemulsions show great promise for a more efficient and effective process to formulate HPMC and poorly water-soluble drugs into highly potent oral films with tunable immediate release.

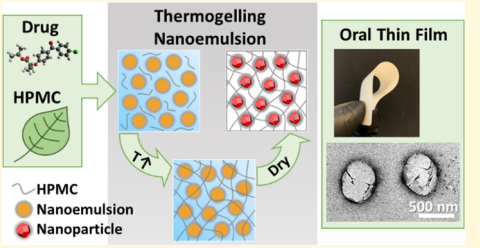

INTRODUCTION

The solubility of drug molecules is a crucial parameter to consider during the design and formulation of new drug products. Nearly 40% of marketed drugs and 90% of drug candidates in the pipeline are poorly water-soluble (i.e., hydrophobic).[1] The hydrophobic nature makes these drugs difficult to be absorbed in the gastrointestinal tract, resulting in limited bioavailability.[2] Among different strategies to overcome the solubility limitation, particle size reduction has gained the most attention for formulation of poorly water-soluble drugs. By reducing the size of hydrophobic drugs to the nanometer range, the dissolution rate of hydrophobic drugs can be significantly improved compared to their bulk counterparts because of the increased surface area and increased saturation solubility.[3,4] However, nanoparticle suspensions are thermodynamically unstable and susceptible to sedimentation, agglomeration, and crystal growth.[5] Moreover, the suspensions are in a liquid form and should be accurately measured and carefully shaken before administration.[6] Motivated by these issues, tremendous efforts have been made to formulate nanoparticles into oral solid dosage forms that possess improved stability and dosage accuracy,[7] such as tablets and capsules. However, these solid dosage forms are considered difficult to swallow by 37% of the population, which can lead to non-adherence and inappropriate drug modifications.[8]

In the past decade, oral films have emerged as a novel solid dosage form that shows great potential over other solid dosage forms for the delivery of poorly water-soluble drugs.[6,9,10] Their large surface area-to-volume ratios enable the rapid dissolution and absorption of drugs in the gastrointestinal tract,[6] leading to significantly increased bioavailability.[9] In addition, they are easy to swallow and thus show exceptional acceptability for geriatric, pediatric, and dysphagic patients.[6,10] In a typical film-forming process, a nanosuspension is first prepared and then mixed with a film-forming polymer solution to form a film precursor for casting and drying.[11−17] Wet stirred media milling is one of the most extensively used techniques to formulate nanoparticle suspensions because it is a robust and well-established process that can be applied to many hydrophobic drugs.[18,19] However, it generally involves long milling durations (3−12 h),[20,21] and the erosion of milling media may cause severe contamination of drugs.[22,23] In addition, irreversible nanoparticle aggregation during long-time processing and drying is still a common problem that can reduce the dissolution rate of drug nanoparticles and negatively affect the drug uniformity in oral films.[14,24] The aggregation problem becomes even more prominent when more drug

Received: March 15, 2022
Revised: May 17, 2022

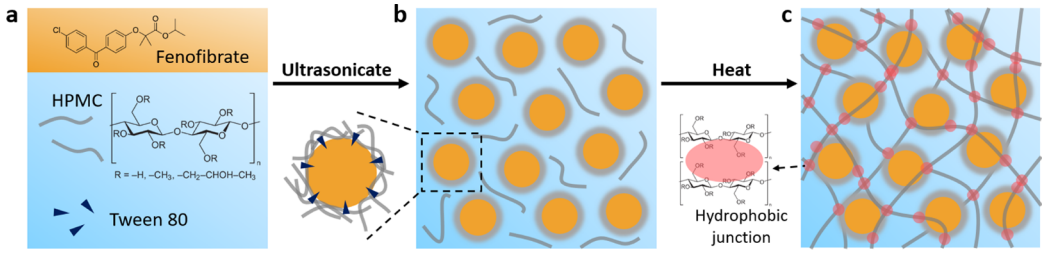

Figure 1. Overview of the thermogelling HPMC nanoemulsion preparation. (a) Dispersed oil phase (saturated fenofibrate-in-anisole solution) and continuous water phase (4 wt % HPMC and a small amount of Tween 80 surfactant). The surfactant-to-oil (SOR) ratio is 1:20. (b) As-prepared thermogelling nanoemulsion after ultrasonication. The nanoemulsion consists of oil nanodroplets that are stabilized by both the HPMC and Tween 80 molecules, which are illustrated as a diffuse halo around the oil nanodroplets. (c) Gel structure formed by the thermogelling nanoemulsion upon heating. The hydrophobic groups of HPMC associate together to form hydrophobic junctions that lead to a gel structure and immobilize the oil nanodroplets. The hydrophobic junctions are illustrated as red points.

nanoparticles are incorporated in oral films,[24] rendering the oral film technology limited to low drug loading capacity.[6,9] Other film-forming technologies involve the incorporation of amorphous solid dispersions[25−27] and solid lipid nanoparticles,[28−30] both of which provide improved bioavailability of poorly water-soluble drugs. However, amorphous solid dispersions are susceptible to recrystallization that undermines the drug efficacy,[25,31] and the recrystallization becomes more significant with increasing drug loadings.[31] Solid lipid nanoparticles also possess stability issues, such as drug expulsion during storage[32] and polymorphic transformation.[30] Therefore, development of an alternative film-forming technology that addresses the above limitations is imperative.

Hydroxypropyl methylcellulose (HPMC) is one of the most prevalent hydrophilic additives in the food and pharmaceutical industries. HPMC is a naturally sourced biopolymer derived from cellulose[33] and is classified as a safe and non-toxic material by the United States Food and Drug Administration (FDA).[34] The non-ionic nature of HPMC ensures reproducible pH-independent drug release profiles in gastrointestinal fluids with varying pH conditions.[35] With many ideal pharmaceutical features, HPMC has become an excellent film-forming polymer for incorporating hydrophobic drug nanoparticles.[11−17] However, formulating HPMC and hydrophobic drugs into oral film products generally requires inefficient and ineffective conventional processes. In addition to inefficient nanoparticle formulations, further mixing of nanoparticle suspensions and a HPMC solution can take another 3−12 h before the mixture is ready for casting.[11−16] Moreover, the mixing can dilute the concentration of drug nanoparticles and compromise the drug loading capacity.[36] Therefore, a more effective and efficient film-forming process needs to be developed based on HPMC. From the material fundamentals, HPMC is a well-known emulsifier that has been used to produce oil-in-water emulsions for hair care[37] and eye drop formulation.[38] In addition, it possesses an interesting thermogelling property[39] that has been applied to form injectable gels for drug delivery.[40] Although these two properties have been widely used to develop liquid dosage forms for delivery of drug, they are generally overlooked in oral film formulations that involve incorporating hydrophobic drugs into a HPMC matrix.

In this work, we report a more efficient and effective film-forming formulation that is enabled by thermogelling HPMC nanoemulsions. We leverage the dual emulsifying and thermogelling properties of HPMC to design the thermogelling nanoemulsions, which provide robust templates to formulate poorly water-soluble drugs into oral films containing drug nanoparticles. HPMC and a surfactant are used to emulsify an oil phase loaded with poorly water-soluble drugs for preparing nanoemulsions. The nanoemulsions are thermogelled because the hydrophobic groups of HPMC can associate together to form a gel network upon heating. The thermally gelled nanoemulsions involve drug-loaded oil nanodroplets that are immobilized in an HPMC hydrogel, which ensures the confined formation of drug nanoparticles in an HPMC matrix. With the proposed mechanism, the thermogelling nanoemulsions can directly act as film precursors to produce oral films with uniform drug nanoparticles embedded in a dried HPMC matrix. To demonstrate the versatility of the proposed formulation, we develop simple predictive rules and correlations to control the oral film thickness for nanoemulsions with different oil weight fractions, which later correspond to different drug loading contents. The efficacy of the proposed approach is supported by electron microscopy and solid-state characterization techniques. The drug nanoparticles are successfully observed, and the most stable solid-state structure is attained after the oral film formation. Moreover, high drug loading contents of the oral films are achieved by increasing the nanoemulsion volume fraction in the precursor solution without the need to modify any other film formulation steps. We also provide evidence that the drug nanoparticles are uniformly distributed in the oral films without irreversible nanoparticle aggregation. For the release performance, the oral films possess a tunable immediate release that has a strong correlation with the film thickness. We present release models to elucidate the release mechanism of the oral films and develop a scaling rule for designing their release profiles. Overall, the developed thermogelling nanoemulsions address many limitations that are still common in conventional film-forming processes, such as inefficient formulation steps, low drug loading capacity, and irreversible nanoparticle aggregation.

RESULTS AND DISCUSSION

Preparation and Thermal Gelation of Thermogelling HPMC Nanoemulsions. Preparing the thermogelling HPMC nanoemulsions requires three key elements: continuous water phase, dispersed oil phase, and surfactant. The continuous water phase is a 4 wt % HPMC aqueous solution (Figure 1a). HPMC molecules are based on a linear polysaccharide cellulose chain with ether-linked methoxy (OCH_3) and hydroxypropyl ($OCH_2CH(OH)CH_3$) side groups. The dispersed oil phase is an anisole solution saturated with

https://doi.org/10.1021/acs.chemmater.2c00801
Chem. Mater. XXXX, XXX, XXX−XXX

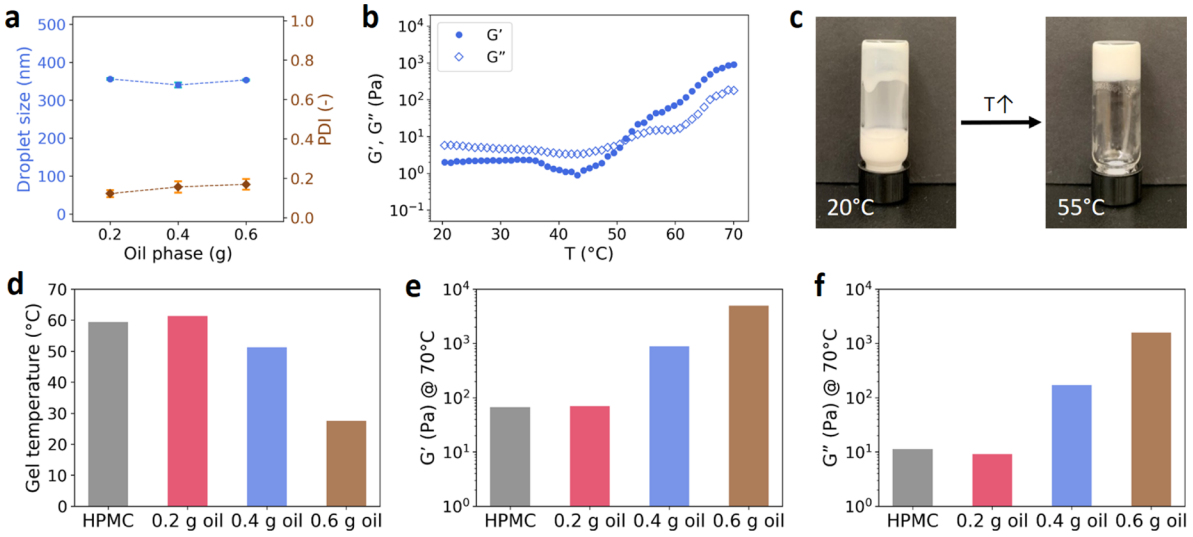

Figure 2. Overview of the nanoemulsion properties. (a) Average droplet sizes (hydrodynamic diameters from DLS) and polydispersity indexes (PDIs) for the thermogelling nanoemulsions with different oil phase masses (0.2, 0.4, and 0.6 g). (b) Elastic modulus (G') and viscous modulus (G'') of the nanoemulsion (0.4 g) in a temperature ramp experiment at a heating rate of 2 °C/min (0.1% strain; 10 rad/s frequency). Apparent gel temperature is defined as the crossover point between G' and G''. (c) Vial inversion test for the nanoemulsion (0.4 g of oil) at temperatures of 20 and 55 °C. (d) Gel temperatures of the pure HPMC (gray bar) and the nanoemulsions with different oil masses (red, blue, and brown bars). (e) Elastic moduli (G') at 70 °C of the pure HPMC (gray bar) and the nanoemulsions with different oil masses (red, blue, and brown bars). (f) Viscous moduli (G'') at 70 °C of the pure HPMC (gray bar) and the nanoemulsions with different oil mass (red, blue, and brown bars).

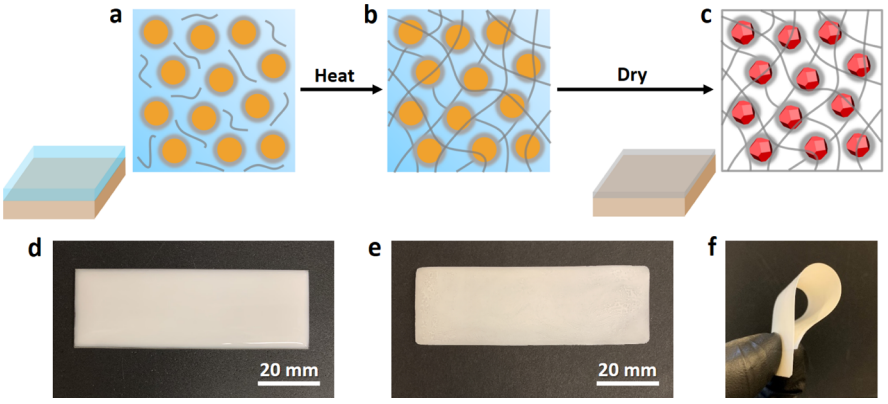

Figure 3. Overview of the film-forming process based on the thermogelling nanoemulsion. (a) Thermogelling nanoemulsion loaded on a glass slide at room temperature. (b) Thermogelling nanoemulsion on a glass slide at 70 °C. The HPMC molecules associate together and form a gel network that immobilizes the oil nanodroplets. (c) Oral film on a glass slide after drying at 70 °C. Drug nanoparticles are induced locally within the oil nanodroplets during drying and are embedded in a dried HPMC matrix after drying. (d) Optical image of the thermogelling nanoemulsion loaded on a glass slide before drying. The dimensions of the glass slide are 75 mm × 25 mm. (e, f) Optical images of the oral film detached from the glass slide after drying. The film condition is 0.4 g of oil, and the thickness is 111.8 μm.

fenofibrate. Fenofibrate is selected as a hydrophobic model drug because of its extremely low water solubility (0.3 μg/mL at 37 °C).[41] Anisole is chosen as an organic solvent because it has a high solubility for hydrophobic fenofibrate and is approved for pharmaceutical formulations. In addition to the HPMC molecules in the water phase, a small amount of Tween 80 surfactant (1/20 of the mass of the oil phase) is added to help emulsify the oil phase. The mixture of all the above materials is vortexed quickly to form a pre-emulsion, which is then placed in an ultrasonicator kept at 10 °C for 30 min. The ultrasonication provides energy to break the large oil droplets into nanoscale droplets. The as-prepared nanoemulsions comprise oil nanodroplets that are uniformly dispersed in the continuous water phase with free HPMC molecules (Figure 1b). These oil nanodroplets are stabilized by both the HPMC and Tween 80 molecules. The nanoemulsions are thermogelling because of the thermoresponsive nature of HPMC. Upon heating, the hydrophobic methoxy groups of HPMC molecules can associate together to form hydrophobic junctions[42−46] as shown by the red points in Figure 1c. The hydrophobic association forms a hydrogel network that immobilizes the oil nanodroplets.

Figure 2a shows the average droplet diameters and polydispersity indexes (PDIs) characterized by dynamic light scattering (DLS) for the thermogelling nanoemulsions with different oil phase mass. With the same 3 g continuous water phase, different mass (0.2, 0.4, and 0.6 g) of the dispersed oil phase and a small amount of Tween 80 (1/20 of the oil mass) are added to prepare the nanoemulsions. The surfactant-to-oil ratio (SOR) is fixed at 1:20 to enable similar nanoemulsion droplet sizes (~350 nm) for different oil mass conditions. The polydispersity indexes (PDIs) of the nanoemulsions vary

https://doi.org/10.1021/acs.chemmater.2c00801
Chem. Mater. XXXX, XXX, XXX−XXX

between 0.1 and 0.2, which lie in the typical range for uniform nanoemulsion droplet sizes.[47,48] To quantify the gel temperatures, temperature ramp experiments are conducted for the pure HPMC and the nanoemulsions (Figure 2b and Supporting Information Figure S1). In addition, the sol−gel transition is qualitatively demonstrated in a vial inversion test (Figure 2c). Figure 2d summarizes the gel temperatures of the pure HPMC and the thermogelling nanoemulsions. Compared to the gel temperature of the pure HPMC (59.4 °C), the nanoemulsion with 0.2 g of oil has a slightly increased gel temperature (61.3 °C). The small change in the gel temperature can be attributed to two competing factors. One is that the oil nanodroplets act as crosslinking points for hydrophobic association upon heating, leading to faster gelation and a lower gel temperature. The other is that amphiphilic Tween 80 molecules can cloak the hydrophobic units of HPMC chains. This cloaking phenomenon delays the gelation and increases the gel temperature because more energy is required to break away the surfactant molecules and expose the hydrophobic groups for association.[49] With the increasing oil mass from 0.2 to 0.6 g, the gel temperature of the nanoemulsion decreases. A higher density of the oil nanodroplets provides more cross-linking points that dominate the cloaking effect of the surfactant, which facilitates hydrophobic association and accelerates gelation upon heating. The elastic moduli and viscous moduli at 70 °C of the pure HPMC and the thermogelling nanoemulsions are summarized in Figure 2e,f. The elastic modulus is higher than the viscous modulus for each condition, indicating solid-like behavior of the gel. The gel becomes stronger with a larger elastic modulus as the oil phase mass increase, because more cross-linking points created by the oil nanodroplets are able to reinforce the gel network.

Preparation of Oral Films with Adjustable Thickness. The proposed film-forming process based on the thermogelling nanoemulsion is shown in Figure 3a−c. A glass slide is first loaded with a layer of the thermogelling nanoemulsion in the sol state at ∼20 °C (Figure 3a,d). The nanoemulsion is then heated to form a gel with immobilized hydrophobic oil nanodroplets (Figure 3b). The heating temperature is chosen to be 70 °C, which is greater than the gel temperatures of the nanoemulsions with different oil phase masses. The drying process then proceeds at the same elevated temperature to evaporate both the water and organic solvent (anisole). During the drying process, the nanoparticles are locally induced within the oil nanodroplets, and the continuous phase hydrogel becomes a dried HPMC matrix (Figure 3c). Because the thermally gelled network protects the oil nanodroplets from coalescence, each nanodroplet is expected to become a single nanoparticle. Therefore, the dried film (i.e., oral film) involves uniform drug nanoparticles embedded in a dried HPMC matrix. The oral film detached from the glass slide has a white appearance, as shown in Figure 3e,f. To demonstrate the advantages of the proposed film-forming process, we summarize the conventional methods for preparing oral films that are loaded with fenofibrate microparticles or nanoparticles in Supporting Information Table S3. The conventional milling methods (wet stirred media milling and fluid energy milling) typically take at least 2 h to mill down solid crystals.[12−15,17] Among the conventional methods, fluid energy milling is difficult to reach the desirable nanoscale range (<1 μm).[12,13] Although melt emulsification provides a faster way to form a nanoparticle suspension (∼15 min), it requires extreme temperatures (melting at 95 °C and sudden cooling to −3 °C for fenofibrate), and it can be difficult to avoid irreversible nanoparticle aggregation during cooling.[11] After a nanoparticle suspension is made using the conventional methods, it has to be mixed with a HPMC film-forming polymer solution to form a film precursor for casting. The mixing process is time-consuming (typically 3−12 h)[11−16] and can compromise the drug loading content because of the dilution effect.[36] In contrast, the film-forming process enabled by the thermogelling nanoemulsions is more efficient and effective. Because the oil droplets are soft, a thermogelling nanoemulsion can be easily formed in 5 min and reach the minimum droplet size in 20 min.[50] Moreover, the thermogelling nanoemulsion can directly act as a film precursor without further mixing with a film-forming polymer.

Because the film formation involves removal of both the water and organic solvent, the solid content (w_{solid}) of the nanoemulsion becomes an important parameter to describe the weight fraction of the non-volatile components after drying, which includes HPMC, fenofibrate, and Tween 80. The solid content (w_{solid}) of the nanoemulsion is described by eq 1, and the result is shown in Figure 4a.

$$w_{solid} = \frac{m_c w_{HPMC} + m_o w_{FEN} + m_{TW}}{m_c + m_o + m_{TW}} \quad (1)$$

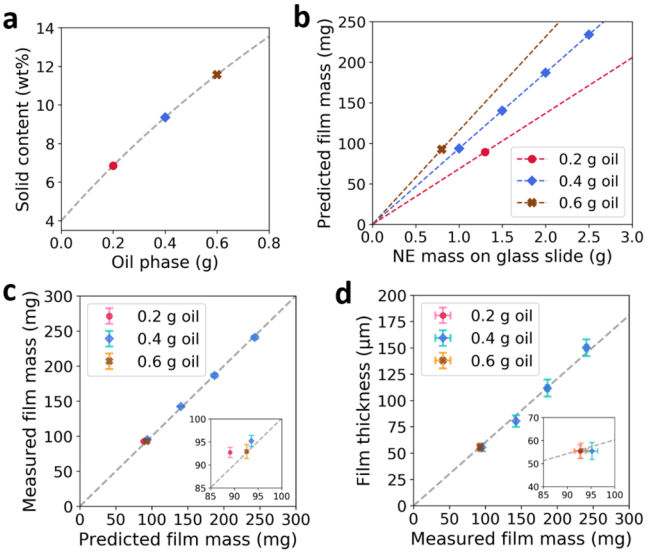

Figure 4. (a) Predicted solid contents from mass balance for the nanoemulsions with different oil phase mass (described by eq 1). The three markers indicate the three compositions chosen in this work. (b) Predicted oral film mass after drying based on the nanoemulsion (NE) mass loaded on the glass slide. The three lines represent the nanoemulsions with three different oil phase mass conditions (described by eq 2). The markers represent the six conditions chosen in this work. (c) Correlation between the predicted oral film mass and the measured oral film mass (R^2 = 0.99). (d) Correlation between the oral film thickness and the measured oral film mass (R^2 = 1.00). From the slope, the densities of the oral films are 0.88 g/cm^3.

where m_c is the mass of the continuous water phase, w_{HPMC} is the HPMC weight fraction in the water phase (4 wt %), m_o is the oil phase mass, and w_{FEN} is the fenofibrate weight fraction in the oil phase (∼45 wt %).[51] Because the oil phase has a high concentration of fenofibrate, a small incremental addition of the oil phase can increase the solid content effectively (∼2.5 wt

https://doi.org/10.1021/acs.chemmater.2c00801
Chem. Mater. XXXX, XXX, XXX−XXX

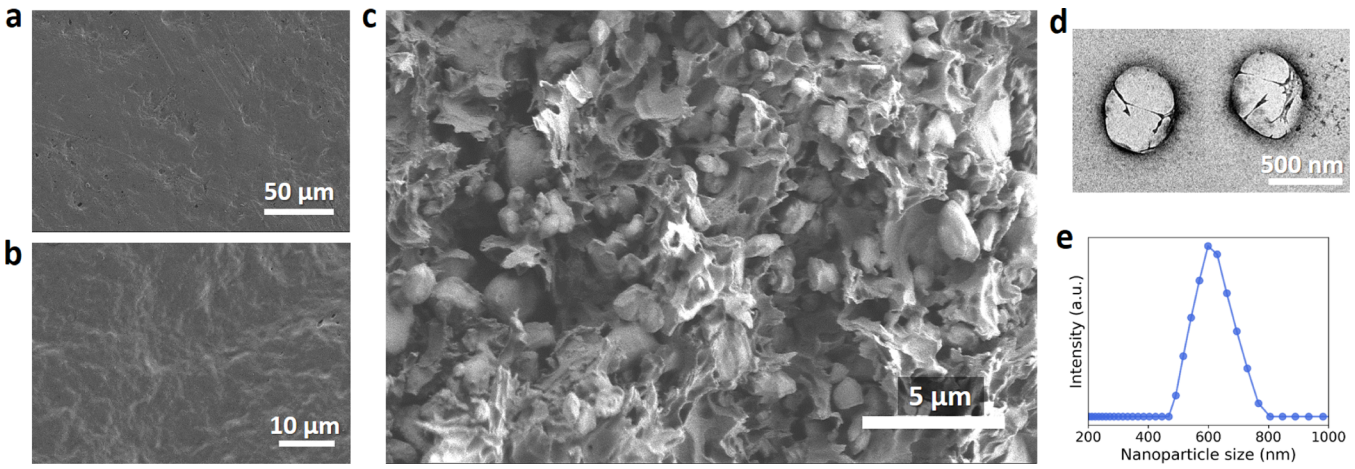

Figure 5. (a, b) SEM images of the oral film surface. (c) SEM image of the oral film cross section (0.4 g of oil; 150.2 μm). The embedded drug nanoparticles have an average diameter of 599.8 ± 71.6 nm. (d) TEM image of the dispersed drug nanoparticles. (e) Size distribution (hydrodynamic diameter) of the dispersed drug nanoparticles determined by dynamic light scattering (DLS). The average diameter and PDI are 597.7 nm and 0.169, respectively.

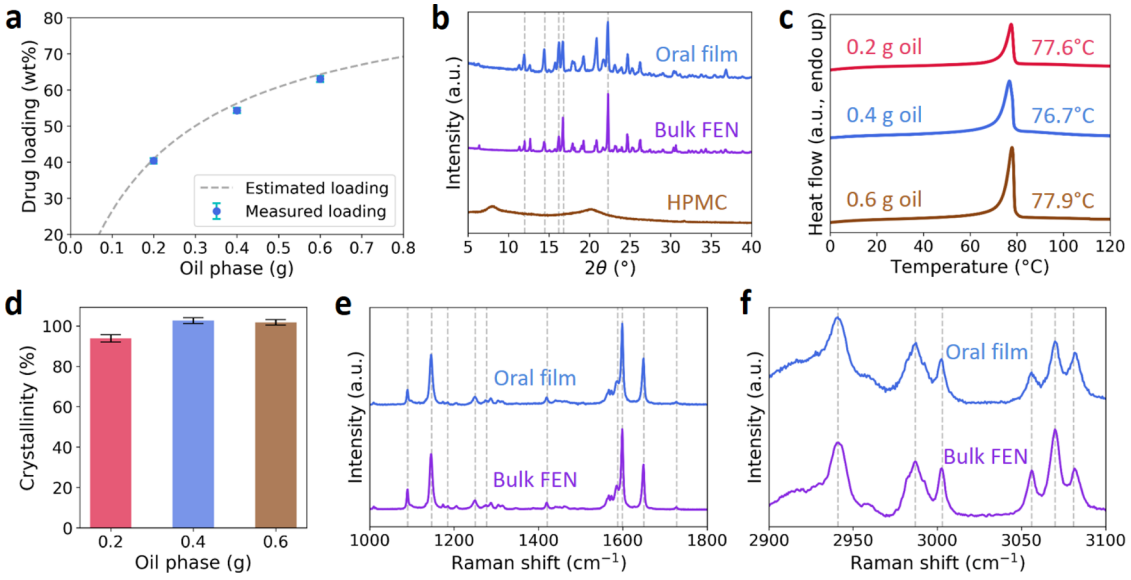

Figure 6. Characterization of the fenofibrate nanoparticles in the oral films. (a) Drug loading content of the oral films as a function of oil phase mass. The estimated drug loading content (gray dashed curve) is described by eq 3. (b) X-ray diffraction (XRD) patterns of the fenofibrate nanoparticles in the oral films, as-received bulk fenofibrate crystals, and HPMC powders. The gray dashed lines correspond to the XRD characteristic peaks for crystalline form I fenofibrate. (c) DSC thermograms and (d) crystallinity of the fenofibrate nanoparticles in the oral films. (e) Raman spectra of the fenofibrate nanoparticles in the oral films with the spectral range between 1000 and 1800 cm^{-1}. (f) Raman spectra of the fenofibrate nanoparticles in the oral films within the spectral range of 2900 to 3100 cm^{-1}. The gray dashed lines in (e) and (f) correspond to the Raman characteristic peaks for crystalline form I fenofibrate.

% increase per 0.2 g of oil addition). With the estimated solid content, the oral film mass is predicted from the mass of the nanoemulsion loaded on a glass slide (Figure 4b). The predicted oral film mass ($m_{\text{dried, p}}$) is expressed as follows:

$$m_{\text{dried,p}} = m_{\text{NE}} w_{\text{solid}} \quad (2)$$

where m_{NE} is the mass of the nanoemulsion loaded on a glass slide. To compare the oral films made from the nanoemulsions with three different oil phase mass conditions, prediction is made for these nanoemulsions to form the oral films with approximately the same mass (~92 mg). To validate the prediction, the oral film mass is measured and compared with the predicted film mass (Figure 4c). The measured film mass agrees well with the predicted film mass. In addition, a good correlation (R^2 = 1.00) is observed between the oral film thickness and the measured oral film mass (Figure 4d). The result suggests that the film thickness is adjustable by varying the mass of the nanoemulsion loaded on the glass slide. The nanoemulsion can be loaded on a glass slide up to 5 g, which corresponds to at least 200 μm for the resulting oral film. The optical images of the oral films for the six conditions are shown in Supporting Information Figure S2.

Characterization of Drug Nanoparticles in Oral Films. The surface and the cross-section of the oral film are observed using scanning electron microscopy (SEM) as shown in Figure 5. A drug-free pure HPMC film is prepared as a control for comparison (Supporting Information Figure S3). For the oral film templated by the nanoemulsion, the surface is flat and

https://doi.org/10.1021/acs.chemmater.2c00801
Chem. Mater. XXXX, XXX, XXX−XXX

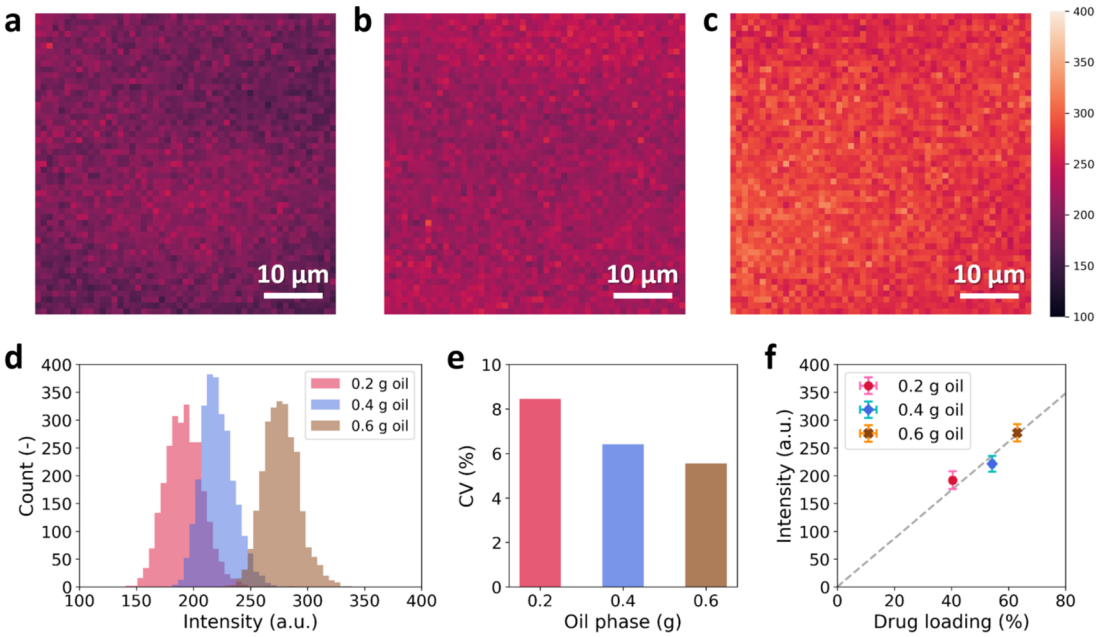

Figure 7. Raman mapping images for the oral films with different oil phase masses: (a) 0.2 g of oil, (b) 0.4 g of oil, and (c) 0.6 g of oil. Color bar values represent Raman peak intensities at 1650 cm^{-1}. The Raman mapping area is 51 μm × 51 μm, and each pixel is 1 μm × 1 μm. (d) Intensity histograms associated with the Raman mapping images in (a) to (c). (e) Coefficients of variation (CV) determined from the intensity histograms. CV represents the ratio of the standard deviation to the mean. (f) Correlation between the intensity and the drug loading content.

does not have distinct nanostructures (Figure 5a,b), which is similar to the case of the pure HPMC film (Supporting Information Figure S3a,b). To observe the cross section, an oblique cut is applied on the films. The cross-sectional images are very different for the nanoemulsion-templated oral film and the pure HPMC film. The pure HPMC film has a flat and smooth cross section (Supporting Information Figure S3c), while the nanoemulsion-templated oral film has evident nanoparticles embedded in the porous HPMC matrix (Figure 5c). The embedded nanoparticles have an average diameter of 599.8 ± 71.6 nm, which is larger than the oil nanoemulsion droplet diameter (~350 nm). The size increase could result from the adsorption of more HPMC molecules to stabilize the drug nanoparticles. To further investigate the ability of the HPMC polymer to stabilize the drug nanoparticles, the oral film is tested for nanoparticle dispersibility in water. In Figure 5d (also Supporting Information Figure S4), the dispersed drug nanoparticles can be directly observed using transmission electron microscopy (TEM), and dynamic light scattering (DLS) shows that the dispersed nanoparticles are stable and have a uniform size distribution (Figure 5e). The average nanoparticle diameter and PDI are 597.7 nm and 0.169, respectively. The above results demonstrate that the thermogelling nanoemulsion can effectively template the formation of uniform drug nanoparticles in the HPMC matrix.

The amount of poorly water-soluble drugs that can be loaded into an oral film is generally limited with conventional film-forming technologies,[6,9] because irreversible aggregation of drug particles can easily occur during processing and drying, especially for oral films with high drug loading contents.[14,24] In contrast, the film-forming process based on the thermogelling nanoemulsion can effectively avoid the aggregation problem because the thermogelling mechanism ensures the confined formation of drug nanoparticles in the immobilized oil nanodroplets. From the aspect of process development, the drug loading content can be easily scaled up by increasing the oil-to-water ratio of the nanoemulsion without any further modifications on the film formulation steps. Adding more oil leads to a higher density of the nanoemulsion droplets, which corresponds to a higher drug nanoparticle density (i.e., higher drug loading content) after drying. Figure 6a shows the drug loading contents of the oral films as a function of the oil phase mass. The measured drug loading contents agree well with the estimated drug loading (ϕ_{FEN}) curve that is predicted by eq 3.

$$\phi_{FEN} = \frac{m_o w_{FEN}}{m_c w_{HPMC} + m_o w_{FEN} + m_{TW}} \quad (3)$$

The high drug loading content is tunable from 40.4 to 63.0 wt % by adding oil from 0.2 to 0.6 g, which is higher than the highest value (37.1 wt %) demonstrated in the prior studies that used conventional methods to prepare oral films loaded with fenofibrate particles (Supporting Information Table S3).[17] In order to monitor the fenofibrate crystal structure before and after the formulation, X-ray diffraction (XRD) patterns are measured for the oral film, as-received bulk fenofibrate crystals, and pure HPMC powders (Figure 6b). The latter two are the starting materials that are dissolved in the dispersed oil and continuous water phases for preparing the nanoemulsions. The nanoparticles in the oral films share the same characteristic peaks of the bulk fenofibrate crystals, which correspond to crystalline form I fenofibrate at the diffraction angles (2θ) of 12, 14.5, 16.2, 16.8, and 22.4°. Form I fenofibrate is a desirable form because it has the highest thermodynamic stability compared to the metastable polymorphs and the amorphous form.[52] The high stability can avoid recrystallization under ambient storage conditions and during dissolution.[51,53] In Figure 6c, differential scanning calorimetry (DSC) identifies a single endothermic peak of melting for the oral films with different oil mass. Compared to the as-received bulk fenofibrate crystals with a melting point of 81.7 °C (Supporting Information Figure S8a), the oral films have melting points of ~77.4 °C (Figure 6c). The melting

https://doi.org/10.1021/acs.chemmater.2c00801
Chem. Mater. XXXX, XXX, XXX−XXX

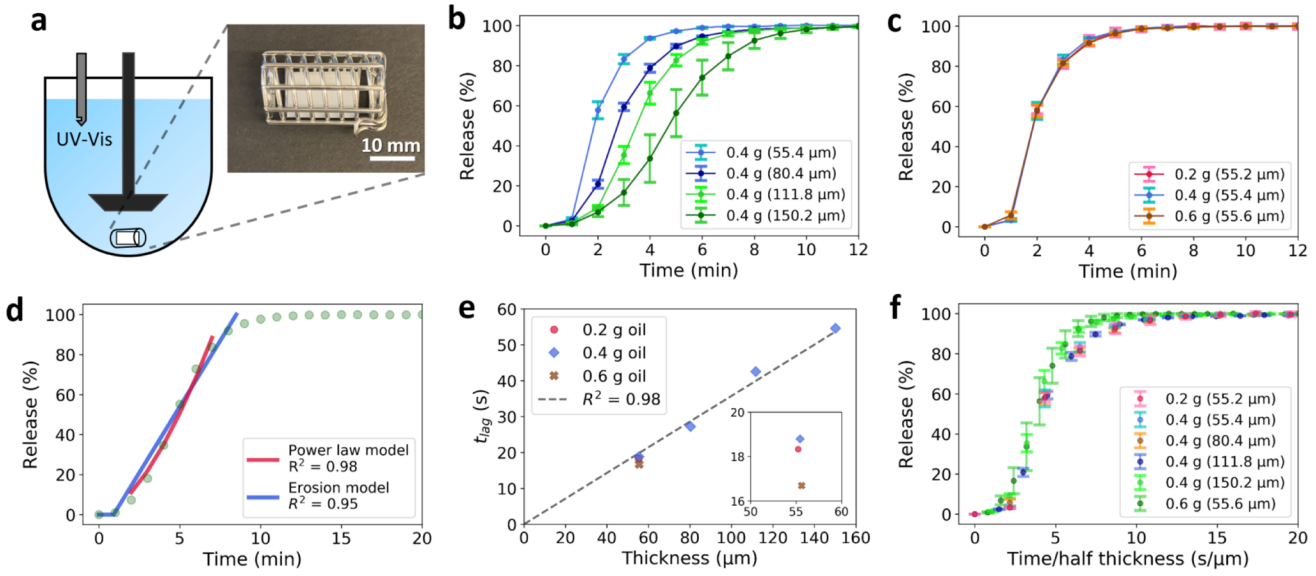

Figure 8. Release profiles and analyses of the oral films. (a) Schematic diagram of the United States Pharmacopeia (USP) Dissolution Apparatus II with an automated UV−Vis probe. The inset photo is a USP compliant sinker basket loaded with an oral film (15 mm × 10 mm). (b, c) Cumulative release profiles for the oral films with different compositions: (b) varying the oil mass with a constant thickness (~55.4 μm) and (c) varying the thickness with a constant oil phase mass (0.4 g oil). (d) Fitting the release profile of the oral film (0.4 g of oil and 150.2 μm) with the power-law model (eq 4) and erosion model (eq 5). (e) Correlation between the lag time (t_{lag}) and the oral film thickness. (f) Rescaling of the release profiles with different compositions onto a universal curve.

point depression is a typical feature of nanocrystals compared to bulk crystals, and the phenomenon can be described by the Gibbs−Thomson equation.[54] The similar decreased melting points of the oral films show that crystalline drug nanoparticles are successfully formed with similar sizes for different oil phase mass, which again supports the effectiveness of using the nanoemulsions as templates. Based on the DSC results, drug crystallinity in the oral films can be estimated with the prior data that correlates the fusion enthalpies and melting points of fenofibrate nanocrystals (see Supporting Information Section S4).[55,56] The estimation shows that the drug in the oral films has a high degree of crystallinity that is close to complete crystallization for different oil mass conditions (Figure 6d). The Raman spectra also suggest that the solid-state form of fenofibrate in the oral film is crystalline form I (Figure 6e,f). The most prominent peaks occur at 1147, 1599, and 1650 (Figure 6e), which correspond to C−O stretching, in-plane benzene ring stretching, and C═O stretching, respectively.[57] Moreover, in the CH-stretching region between 2900 and 3100 cm^{-1} (Figure 6f), there are three peaks between 3050 and 3100, which are fingerprints for crystalline form I fenofibrate.[57]

To investigate the uniformity of the drug nanoparticles in the oral films, Raman mapping images are taken for the oral films with different oil masses (Figure 7a−c). The Raman intensity becomes higher (i.e., brighter color according to the heat map) as the oil mass increases, which corresponds to a higher density of fenofibrate nanoparticles in the oral film. In addition, no aggregation of pixels (1 μm × 1 μm) is observed from the Raman mapping images, indicating that the fenofibrate nanoparticles are uniformly distributed in the film. Figure 7d shows the intensity histograms associated with the images in Figure 7a−c. The average intensity increases with increasing oil mass, and the standard deviation is similar for different oil mass (~15 au). In Figure 7e, the coefficients of variation (CV) for different oil masses are further calculated, which are 8.5, 6.4, and 5.6% for 0.2, 0.4, and 0.6 g of oil, respectively. The CV value becomes smaller as the drug loading content increases, which is consistent with a previous finding that increasing the density of nanostructures can enhance the Raman signal uniformity.[58] To set a benchmark, for highly uniform nanostructure arrays reported in previous studies, the CV values of the Raman mapping signals typically lie between 4.3 and 14.8%.[58−60] This quantitatively supports that the oral films templated by the thermogelling nanoemulsions have a high drug content uniformity. The average Raman intensity is roughly proportional to the drug loading content (Figure 7f), which is consistent with a previous result that the Raman signal of a drug product is linearly correlated with the drug concentration.[61]

Release Profiles of Oral Films. Fenofibrate belongs to Biopharmaceutics Classification System (BCS) Class II drugs that have high permeability and low solubility.[62] This means that absorption of dissolved fenofibrate is much faster than fenofibrate dissolution, causing sink conditions to prevail in vivo. A 25 mM sodium dodecyl sulfate (SDS) aqueous solution recommended by the FDA[63] is used to simulate in vivo solubilization by biorelevant surfactants[64] and create a sink condition during the dissolution, which provides a good proxy of in vivo condition.[65,66] As suggested in the literature, a sinker basket is used to load and transfer the oral film (Figure 8a).[67] This can prevent the oral film from floating or sticking to the paddle or the vessel wall. To deconvolute the effects of drug loading content and thickness, we first studied the release profiles for the oral films with the same oil mass (0.4 g) and different thickness. Figure 8b shows that varying the oral film thickness leads to different release profiles. It takes longer time to finish the release as the oral film thickness increases (Figure 8b). In contrast to the as-received bulk fenofibrate crystals (~240 μm), which takes as long as ~12 h to reach the first 80% release (Supporting Information Figure S10a), the oral films exhibit a tunable immediate release (>80% release in 7

https://doi.org/10.1021/acs.chemmater.2c00801
Chem. Mater. XXXX, XXX, XXX−XXX

min and ∼100% release in 11 min for all conditions). The fast release rates are attributed to the large surface-to-volume ratios of the oral films and the successful formation of drug nanoparticles. The surface-to-volume ratios of the oral films can achieve 133 to 361 cm^2/cm^3 for the film thickness range between 55.4 and 150.2 μm, which are much larger than the values of ∼10 cm^2/cm^3 for drug tablets.[68,69] Then, the release profiles for the oral films with the same thickness (∼55.4 μm) and different oil phase mass are compared (Figure 8c). The release profiles are nearly identical, indicating that the release does not depend on the drug loading content at the same thickness. In addition, the thin films (∼55.4 μm) possess a large surface-to-volume ratio to achieve very fast release rates—3 min to reach 80% release and another 4 min to complete the release. In prior studies, irreversible nanoparticle aggregation can easily lead to a distinct reduction of the release rate[70,71] because the improved dissolution resulting from the high surface area of the nanoparticles is lost. In this work, the same fast release rates for different oil mass provide evidence that irreversible nanoparticle aggregation is not a problem when the drug loading content is increased. To elucidate the release mechanism of the oral films, a power-law model is first used to fit the release profiles (as the red curve in Figure 8d):[72]

$$\frac{M_t}{M_\infty} = kt^n \tag{4}$$

where M_t and M_∞ are the amount of drug released at time t and infinite time, k is the kinetic constant (with the unit of t^{-n}), and n is the diffusional exponent that indicates the drug release mechanism. From the fitting results (Supporting Information Figure S11a–f), the exponent n values are greater than 1.4 for all the release profiles (Supporting Information Figure S11g), suggesting that the drug release from the oral film is erosion-controlled.[73] Our observations also indicate that the film matrix erodes over time, and the release is complete once the oral film is fully dissolved. The erosion-controlled mechanism indicates that the dissolution of drug nanoparticles is as fast as the film erosion, and poor dissolution of hydrophobic fenofibrate is no longer a rate-limiting barrier for the drug release. To further analyze the release kinetics, an erosion model for a thin film (half thickness = a) expressed by eq 5 is used to determine the erosion constant (k_e, with the unit of m/s) and lag time (t_{lag})[74] as the blue curve in Figure 8d (see the details in Supporting Information Section S7).

$$\frac{M_t}{M_\infty} = \frac{k_e(t - t_{lag})}{a} \tag{5}$$

The lag time is introduced to account for release suppression due to the initial wetting of the oral film when it first contacts the release medium.[75] In Figure 8e, the lag time (t_{lag}) is proportional to the film thickness ($2a$), which can be explained by the fact that a thinner film has a larger surface-to-volume ratio for faster water hydration before the erosion plays an important role. Because the erosion constants (k_e) are similar for different oral film conditions (Supporting Information Figure S12g) and the lag time is proportional to the film thickness (Figure 8e), a scaling behavior is found mathematically between the fractional release $\frac{M_t}{M_\infty}$ and the $\frac{t}{a}$ (see Supporting Information Section S8). With the scaling rule, the release profiles for various conditions can be collapsed into one master curve (Figure 8f), which provides a simple design rule for engineering the release profiles of oral films.

CONCLUSIONS

We have developed thermogelling HPMC nanoemulsions as robust templates to formulate poorly water-soluble drugs into oral films containing drug nanoparticles. The thermogelling nanoemulsions are prepared using HPMC and Tween 80 to emulsify saturated fenofibrate-in-anisole solution. The nanoemulsions can gelate upon heating with the hydrophobic groups of HPMC associating together to form hydrophobic junctions, which lead to a hydrogel network with immobilized oil nanodroplets. In contrast to inefficient conventional film-forming processes, the thermogelling nanoemulsions can directly act as film precursors for casting and drying. The thermally gelled nanoemulsions can effectively template the formation of uniform drug nanoparticles in a dried HPMC matrix to produce oral films. The oral film thickness is predictable and adjustable by varying the mass of the nanoemulsion loaded on a glass substrate. The uniform drug nanoparticles (∼600 nm) in the oral films have been successfully observed using SEM, TEM, and DLS. The proposed film-forming technology enables a tunable high drug loading content of the oral films up to 63 wt % without any further modifications on the film formulation steps. After the oral film formulation, the most stable crystalline form I fenofibrate is attained as validated by XRD, Raman spectroscopy, and DSC analyses. The melting point depression for the fenofibrate in the oral films demonstrates the formation of crystalline drug nanoparticles. Raman mapping results further show that the oral films have high drug content uniformity. In the release tests, the oral films display a tunable immediate release because the films have large surface-area-to-volume ratios and the drug nanoparticles are fast-dissolving. Moreover, increasing the drug loading content at the same film thickness does not affect the release profiles, which supports that irreversible nanoparticle aggregation is not a problem even when the high drug loading content is achieved. Finally, we present that the drug release from the oral film is erosion-controlled, indicating that the drug dissolution has been significantly improved and is no longer a rate-limiting step. Based on the erosion mechanism, a scaling rule is developed to provide simple design rule for engineering the release profiles of oral films. Overall, the thermogelling nanoemulsions enable a more efficient and effective film-forming process to formulate HPMC and poorly water-soluble drugs into oral films with high drug loading capacity. For the future work, the thermogelling HPMC nanoemulsion is expected to template different polymorphs of a poorly water-soluble drug because the nanoemulsion can provide independent controls of different factors for drug polymorph controls, such as surfactant addition,[76] solvent choices,[77] solvent evaporation rates,[78] and confinement.[77]

EXPERIMENTAL SECTION

Materials. Hydroxypropyl methylcellulose (HPMC, viscosity of 40–60 cP for 2 wt % in H_2O at 20 °C, molecular weight of ∼22,000 g/mol, methoxyl content of 28–30%, hydroxypropoxyl content of 7–12%), Tween 80 (polysorbate), fenofibrate, anisole, ethanol, and sodium dodecyl sulfate (SDS) were purchased from Sigma-Aldrich and used without further purification steps.

Preparation of Thermogelling HPMC Nanoemulsions. The thermogelling HPMC nanoemulsions consist of a continuous water

https://doi.org/10.1021/acs.chemmater.2c00801
Chem. Mater. XXXX, XXX, XXX−XXX

phase and a dispersed phase oil phase. The continuous water phase was a 4 wt % HPMC aqueous solution. The dispersed oil phase was a saturated fenofibrate-in-anisole solution, which was prepared by adding bulk fenofibrate crystals into anisole until excessive crystals could not be further dissolved and settled down at the bottom. To prepare the nanoemulsions, a pre-emulsion was first prepared by vortexing a mixture of the continuous phase, dispersed phase, and Tween 80 in a 50 mL Falcon conical centrifuge tube. The nanoemulsion compositions for different oil phase mass are summarized in Supporting Information Table S1. The surfactant-to-oil (SOR) ratio was fixed at 1:20 to fix the nanoemulsion droplet size. The pre-emulsion was then ultrasonicated at a 30% amplitude in an ultrasonicator with a 24 mm diameter horn (from Cole Parmer) at a frequency of 20 kHz for 30 min. A cooling circulating water bath was used to keep the ultrasonicator at 10 °C.

Dynamic Light Scattering. The droplet sizes and polydispersity indexes (PDIs) of the nanoemulsions were measured by dynamic light scattering (Brookhaven NanoBrook 90Plus PALS), which was operated at a fixed scattering angle of 90° and a temperature of 25 °C. The sample was prepared by diluting 5 μL of the nanoemulsion solution with 3 mL of deionized water in a cuvette. The dilution is performed to avoid multiple scattering effects and ensure a consistent baseline. For each sample, five sets of 1 min measurements were done to determine the nanoemulsion size distribution.

Rheological Characterization of Thermogelling Nanoemulsions. The rheological properties of the nanoemulsions were characterized using a stress-controlled rheometer (DHR-3, TA instrument) equipped with a plate geometry (diameter = 40 mm and gap = 500 μm) and a temperature-controlled Peltier lower-plate. To minimize the evaporation, a small amount of water was added on top of the cone geometry, and a solvent trap was used. Before each measurement, a conditioning procedure was performed: a pre-shear at a constant rotational speed of 10 rad/s for 60 s at 20 °C, followed by an equilibration for 60 s at 20 °C. Temperature ramp measurements were conducted from 20 to 70 °C with a heating rate of 2 °C/min, a strain amplitude of 0.1%, and frequency of 10 rad/s.

Preparation of Oral Films. A microscope slide (plain glass, VWR VistaVision) with dimensions of 75 mm × 25 mm × 1 mm (length × width × height) was used a substrate for oral film formulation. The thermogelling nanoemulsion was poured on a glass slide, and the required nanoemulsion masses for different conditions to achieve the targeted thickness are summarized in Supporting Information Table S2. Then, the glass slide carrying a layer of the nanoemulsion was quickly transferred to a 70 °C oven and dried overnight to evaporate the anisole and water. After drying, an oral film was detached from the glass slide and stored at room temperature for further characterization and release tests.

Film Thickness Measurement. The thickness of the oral films was measured using a digimatic micrometer (series no. 293, Mitutoyo) with an accuracy of 0.001 mm. Thickness values were measured at 10 different locations across each oral film and used to calculate the average and standard deviation.

Scanning Electron Microscopy. The surface and cross section of the oral films were observed using a high-resolution scanning electron microscope (Zeiss HRSEM) at an accelerating voltage of 1.3 kV. All samples were prepared on SEM specimen stubs with carbon tape. The SEM images were analyzed with ImageJ to estimate the drug nanoparticle size.

Transmission Electron Microscopy. Observation of the dispersed nanoparticles from the oral films was carried out using an FEI Tecnai G2 Spirit TWIN TEM equipped with a LaB6 filament and operating at an accelerating voltage of 120 kV. The dispersed nanoparticle suspension was drop-cast onto a carbon film supported copper grid (size 200 mesh), and bright-field microscopy images were taken using a Gatan CCD camera.

Drug Loading Measurement. The drug loadings of the oral films were determined using a UV−Vis spectrophotometer (Thermo Scientific NanoDrop One). According to the UV−Vis absorbance spectrum from 150 to 850 nm (Supporting Information Figure S7a), the absorbance peak occurs at λ = 287 nm for the carbonyl groups of fenofibrate. A concentration−absorbance calibration curve was developed using fenofibrate-in-ethanol solutions with different concentrations ranging from 0.01 to 0.5 mg/mL at λ = 287 nm (Supporting Information Figure S7b). For drug loading content measurements, a 10 mg small piece of the oral film was soaked in 3 mL of ethanol and vortexed for 1 min. The ethanol solution was sampled and diluted 10 times to lie in the range of the calibration curve for UV−Vis measurements. All measurements were done in triplicate.

X-Ray Diffraction Analysis. The crystal structures of the as-received bulk fenofibrate crystals and the fenofibrate nanoparticles in the oral films were characterized by XRD using an in reflection mode (Philips PANalytical X'Pert Pro MPD). The oral film was ground and placed on a silicon crystal zero diffraction plate. The X-ray source was generated using a copper anode (K_α emission wavelength of 1.54 Å) at 40 kV and 40 mA. The diffraction angle 2θ was swept from 4 to 40° with a step size of 0.01671° at a scanning rate of 2°/min.

Differential Scanning Calorimetry Analysis. The melting points of the as-received bulk fenofibrate crystals and the fenofibrate nanoparticles in the oral films were determined using a differential scanning calorimeter (TA Instruments Q2000). An inert environment was maintained in the sample chamber with nitrogen flowing at 50 mL/min. For each measurement, a set of a Tzero pan and lid was used with ∼5 mg of the ground oral film. A temperature ramp was performed from −10 to 150 °C at a heating rate of 10 °C/min.

Raman Spectroscopy. Raman spectroscopy was performed using a Horiba Jobin Yvon LabRAM HR800 system that involves a 633 nm excitation laser, 100× objective lens, and 1800 lines per mm grating. Prior to the measurement, the system was calibrated using the standard 521 cm^{-1} band of Si. The Raman spectra were analyzed using the LabSpec 5 software. The baseline correction of the spectra was implemented using a line with a degree of two. Raman mapping was performed at a step increment of 1 μm in both x and y directions over 51 μm × 51 μm area of the oral film. The Raman mapping was based on the signal at 1650 cm^{-1}.

Tensile Testing. Tensile properties of the oral films were measured using an Instron 8848 MicroTester. Each oral film was first glued onto a hollow cardboard using 5 min epoxy. The gauge length and width of the thin film were 14 and 5 mm, respectively. The cardboard with the oral film was then held between the two clamps, and the connecting parts of the cardboard were cut. The tensile testing was performed at a constant crosshead displacement rate of 0.005 mm/s until the point of film fracture. A stress−strain curve was obtained for each oral film. The stress (engineering stress) was calculated by normalizing the tensile force over the initial cross-sectional area of the oral film. The strain (engineering strain) was calculated by dividing the difference between the initial and final lengths by the initial length of the oral film. From the stress−strain curve, the tensile strength and the elongation at break were obtained from the maximum stress and the strain corresponding to the maximum stress. The Young's modulus was obtained from the initial elastic deformation region of the stress−strain curve.

Drug Release Experiment. The release profiles of the oral films were measured using a USP Dissolution Apparatus II (Agilent Technologies Varian VK 7025). Integrated in the dissolution apparatus, a Cary 50 UV−vis spectrometer and an in situ probe set automatically recorded the absorbance at a wavelength of 287 nm every minute. The release medium was a 900 mL of 25 mM sodium dodecyl sulfate (SDS) aqueous solution, which is recommended by the FDA Dissolution Methods Database for fenofibrate dosage forms[63] to simulate in vivo solubilization of hydrophobic fenofibrate by biorelevant surfactants.[64−66] Each oral film (15 mm × 10 mm) was placed into a USP-compliant Japanese Pharmacopeia sinker basket to decrease the variability of the release results caused by potential floating of the oral films.[67] The operating temperature and paddle rotational speed were set at 37 °C and 75 rpm, respectively. The release experiment for each sample was done in triplicate.

https://doi.org/10.1021/acs.chemmater.2c00801
Chem. Mater. XXXX, XXX, XXX−XXX

■ ASSOCIATED CONTENT

Supporting Information

The Supporting Information is available free of charge at https://pubs.acs.org/doi/10.1021/acs.chemmater.2c00801.

Parameter space for the thermogelling nanoemulsions and oral films; supporting figures for the thermogelling nanoemulsions and oral films; supporting drug loading data; estimation of fenofibrate crystallinity in oral film; tensile testing; supporting release data; and erosion model for oral films (PDF)

■ AUTHOR INFORMATION

Corresponding Author

Patrick S. Doyle − *Department of Chemical Engineering, Massachusetts Institute of Technology, Cambridge, Massachusetts 02139, United States; Campus for Research Excellence and Technological Enterprise, 138602 Singapore, Singapore;* orcid.org/0000-0003-2147-9172; Email: pdoyle@mit.edu

Author

Liang-Hsun Chen − *Department of Chemical Engineering, Massachusetts Institute of Technology, Cambridge, Massachusetts 02139, United States*

Complete contact information is available at: https://pubs.acs.org/10.1021/acs.chemmater.2c00801

Notes

The authors declare no competing financial interest.

■ ACKNOWLEDGMENTS

This research was supported by NSF grant CMMI-1824297.

■ REFERENCES

(1) Loftsson, T.; Brewster, M. E. Pharmaceutical Applications of Cyclodextrins: Basic Science and Product Development. *J. Pharm. Pharmacol.* **2010**, *62*, 1607−1621.

(2) Kesisoglou, F.; Panmai, S.; Wu, Y. Nanosizing - Oral Formulation Development and Biopharmaceutical Evaluation. *Adv. Drug Delivery Rev.* **2007**, *59*, 631−644.

(3) Junghanns, J.-U. A. H.; Müller, R. H. Nanocrystal Technology, Drug Delivery and Clinical Applications. *Int. J. Nanomed.* **2008**, *3*, 295−309.

(4) Junyaprasert, V. B.; Morakul, B. Nanocrystals for Enhancement of Oral Bioavailability of Poorly Water-Soluble Drugs. *Asian J. Pharm. Sci.* **2015**, *10*, 13−23.

(5) Wu, L.; Zhang, J.; Watanabe, W. Physical and Chemical Stability of Drug Nanoparticles. *Adv. Drug Delivery Rev.* **2011**, *63*, 456−469.

(6) Borges, A. F.; Silva, C.; Coelho, J. F. J.; Simões, S. Oral Films: Current Status and Future Perspectives: I-Galenical Development and Quality Attributes. *J. Controlled Release* **2015**, *206*, 1−19.

(7) Scoutaris, N.; Ross, S. A.; Douroumis, D. 3D Printed "Starmix" Drug Loaded Dosage Forms for Paediatric Applications. *Pharm. Res.* **2018**, *35*, 34.

(8) Schiele, J. T.; Quinzler, R.; Klimm, H. D.; Pruszydlo, M. G.; Haefeli, W. E. Difficulties Swallowing Solid Oral Dosage Forms in a General Practice Population: Prevalence, Causes, and Relationship to Dosage Forms. *Eur. J. Clin. Pharmacol.* **2013**, *69*, 937−948.

(9) Dixit, R. P.; Puthli, S. P. Oral Strip Technology: Overview and Future Potential. *J. Controlled Release* **2009**, *139*, 94−107.

(10) Karki, S.; Kim, H.; Na, S. J.; Shin, D.; Jo, K.; Lee, J. Thin Films as an Emerging Platform for Drug Delivery. *Asian J. Pharm. Sci.* **2016**, *11*, 559−574.

(11) Bhakay, A.; Vizzotti, E.; Li, M.; Davé, R.; Bilgili, E. Incorporation of Fenofibrate Nanoparticles Prepared by Melt Emulsification into Polymeric Films. *J. Pharm. Innovation* **2016**, *11*, 53−63.

(12) Zhang, L.; Aloia, M.; Pielecha-Safira, B.; Lin, H.; Rajai, P. M.; Kunnath, K.; Davé, R. N. Impact of Superdisintegrants and Film Thickness on Disintegration Time of Strip Films Loaded With Poorly Water-Soluble Drug Microparticles. *J. Pharm. Sci.* **2018**, *107*, 2107−2118.

(13) Zhang, L.; Li, Y.; Abed, M.; Davé, R. N. Incorporation of Surface-Modified Dry Micronized Poorly Water-Soluble Drug Powders into Polymer Strip Films. *Int. J. Pharm.* **2018**, *535*, 462−472.

(14) Sievens-Figueroa, L.; Bhakay, A.; Jerez-Rozo, J. I.; Pandya, N.; Romañach, R. J.; Michniak-Kohn, B.; Iqbal, Z.; Bilgili, E.; Davé, R. N. Preparation and Characterization of Hydroxypropyl Methyl Cellulose Films Containing Stable BCS Class II Drug Nanoparticles for Pharmaceutical Applications. *Int. J. Pharm.* **2012**, *423*, 496−508.

(15) Krull, S. M.; Susarla, R.; Afolabi, A.; Li, M.; Ying, Y.; Iqbal, Z.; Bilgili, E.; Davé, R. N. Polymer Strip Films as a Robust, Surfactant-Free Platform for Delivery of BCS Class II Drug Nanoparticles. *Int. J. Pharm.* **2015**, *489*, 45−57.

(16) Zhang, J.; Ying, Y.; Pielecha-Safira, B.; Bilgili, E.; Ramachandran, R.; Romañach, R.; Davé, R. N.; Iqbal, Z. Raman Spectroscopy for In-Line and off-Line Quantification of Poorly Soluble Drugs in Strip Films. *Int. J. Pharm.* **2014**, *475*, 428−437.

(17) Kevadiya, B. D.; Barvaliya, M.; Zhang, L.; Anovadiya, A.; Brahmbhatt, H.; Paul, P.; Tripathi, C. Fenofibrate Nanocrystals Embedded in Oral Strip-Films for Bioavailability Enhancement. *Bioengineering* **2018**, *5*, 16.

(18) Merisko-Liversidge, E.; Liversidge, G. G.; Cooper, E. R. Nanosizing: A Formulation Approach for Poorly-Water-Soluble Compounds. *Eur. J. Pharm. Sci.* **2003**, *18*, 113−120.

(19) Bhakay, A.; Rahman, M.; Dave, R. N.; Bilgili, E. Bioavailability Enhancement of Poorly Water-Soluble Drugs via Nanocomposites: Formulation−Processing Aspects and Challenges. *Pharmaceutics* **2018**, *10*, 86.

(20) Loh, Z. H.; Samanta, A. K.; Sia Heng, P. W. Overview of Milling Techniques for Improving the Solubility of Poorly Water-Soluble Drugs. *Asian J. Pharm. Sci.* **2014**, *10*, 255−274.

(21) Shah, D. A.; Murdande, S. B.; Dave, R. H. A Review: Pharmaceutical and Pharmacokinetic Aspect of Nanocrystalline Suspensions. *J. Pharm. Sci.* **2016**, *105*, 10−24.

(22) Juhnke, M.; Märtin, D.; John, E. Generation of Wear during the Production of Drug Nanosuspensions by Wet Media Milling. *Eur. J. Pharm. Biopharm.* **2012**, *81*, 214−222.

(23) Li, M.; Yaragudi, N.; Afolabi, A.; Dave, R.; Bilgili, E. Sub-100nm Drug Particle Suspensions Prepared via Wet Milling with Low Bead Contamination through Novel Process Intensification. *Chem. Eng. Sci.* **2015**, *130*, 207−220.

(24) Krull, S. M.; Moreno, J.; Li, M.; Bilgili, E.; Davé, R. N. Critical Material Attributes (CMAs) of Strip Films Loaded with Poorly Water-Soluble Drug Nanoparticles: III. Impact of Drug Nanoparticle Loading. *Int. J. Pharm.* **2017**, *523*, 33−41.

(25) Prodduturi, S.; Manek, R. V.; Kolling, W. M.; Stodghill, S. P.; Repka, M. A. Solid-State Stability and Characterization of Hot-Melt Extruded Poly(Ethylene Oxide) Films. *J. Pharm. Sci.* **2005**, *94*, 2232−2245.

(26) Panraksa, P.; Jantrawut, P.; Tipduangta, P.; Jantanasakulwong, K. Formulation of Orally Disintegrating Films as an Amorphous Solid Solution of a Poorly Water-Soluble Drug. *Membranes* **2020**, *10*, 1−17.

(27) Weuts, I.; Van Dycke, F.; Voorspoels, J.; De Cort, S.; Stokbroekx, S.; Leemans, R.; Brewster, M. E.; Xu, D.; Segmuller, B.; Turner, Y. T. A. Physicochemical Properties of the Amorphous Drug, Cast Films, and Spray Dried Powders to Predict Formulation Probability of Success for Solid Dispersions: Etravirine. *J. Pharm. Sci.* **2011**, *100*, 260−274.

(28) Steiner, D.; Emmendörffer, J. F.; Bunjes, H. Orodispersible Films: A Delivery Platform for Solid Lipid Nanoparticles? *Pharmaceutics* **2021**, *13*, 2162.

(29) Jones, E.; Ojewole, E.; Kalhapure, R.; Govender, T. In Vitro Comparative Evaluation of Monolayered Multipolymeric Films

Embedded with Didanosine-Loaded Solid Lipid Nanoparticles: A Potential Buccal Drug Delivery System for ARV Therapy. *Drug Dev. Ind. Pharm.* **2014**, *40*, 669−679.
(30) Ghasemiyeh, P.; Mohammadi-Samani, S. Solid Lipid Nanoparticles and Nanostructured Lipid Carriers as Novel Drug Delivery Systems: Applications, Advantages and Disadvantages. *Res Pharm Sci.* **2018**, *13*, 288−303.
(31) Serajuddln, A. T. M. Solid Dispersion of Poorly Water-Soluble Drugs: Early Promises, Subsequent Problems, and Recent Breakthroughs. *J. Pharm. Sci.* **1999**, *88*, 1058−1066.
(32) Shirodkar, R. K.; Kumar, L.; Mutalik, S.; Lewis, S. Solid Lipid Nanoparticles and Nanostructured Lipid Carriers: Emerging Lipid Based Drug Delivery Systems. *Pharm. Chem. J.* **2019**, *53*, 440−453.
(33) Cao, Y.; Mezzenga, R. Design Principles of Food Gels. *Nat. Food* **2020**, *1*, 106−118.
(34) Li, C. L.; Martini, L. G.; Ford, J. L.; Roberts, M. The Use of Hypromellose in Oral Drug Delivery. *J. Pharm. Pharmacol.* **2010**, *57*, 533−546.
(35) Asare-Addo, K.; Conway, B. R.; Larhrib, H.; Levina, M.; Rajabi-Siahboomi, A. R.; Tetteh, J.; Boateng, J.; Nokhodchi, A. The Effect of PH and Ionic Strength of Dissolution Media on In-Vitro Release of Two Model Drugs of Different Solubilities from HPMC Matrices. *Colloids Surf., B* **2013**, *111*, 384−391.
(36) Steiner, D.; Finke, J. H.; Kwade, A. Efficient Production of Nanoparticle-Loaded Orodispersible Films by Process Integration in a Stirred Media Mill. *Int. J. Pharm.* **2016**, *511*, 804−813.
(37) Nazir, H.; Zhang, W.; Liu, Y.; Chen, X.; Wang, L.; Naseer, M. M.; Ma, G. Silicone Oil Emulsions: Strategies to Improve Their Stability and Applications in Hair Care Products. *Int. J. Cosmet. Sci.* **2014**, *36*, 124−133.
(38) Schulz, M. B.; Daniels, R. Hydroxypropylmethylcellulose (HPMC) as Emulsifier for Submicron Emulsions: Influence of Molecular Weight and Substitution Type on the Droplet Size after High-Pressure Homogenization. *Eur. J. Pharm. Biopharm.* **2000**, *49*, 231−236.
(39) Joshi, S. C. Sol-Gel Behavior of Hydroxypropyl Methylcellulose (HPMC) in Ionic Media Including Drug Release. *Materials* **2011**, *4*, 1861−1905.
(40) Okubo, M.; Iohara, D.; Anraku, M.; Higashi, T.; Uekama, K.; Hirayama, F. A Thermoresponsive Hydrophobically Modified Hydroxypropylmethylcellulose/Cyclodextrin Injectable Hydrogel for the Sustained Release of Drugs. *Int. J. Pharm.* **2020**, *575*, No. 118845.
(41) Vogt, M.; Kunath, K.; Dressman, J. B. Dissolution Enhancement of Fenofibrate by Micronization, Cogrinding and Spray-Drying: Comparison with Commercial Preparations. *Eur. J. Pharm. Biopharm.* **2008**, *68*, 283−288.
(42) Bonetti, L.; De Nardo, L.; Farè, S. Thermo-Responsive Methylcellulose Hydrogels: From Design to Applications as Smart Biomaterials. *Tissue Eng., Part B* **2021**, *27*, 486−513.
(43) Haque, A.; Morris, E. R. Thermogelation of Methylcellulose. Part I: Molecular Structures and Processes. *Carbohydr. Polym.* **1993**, *22*, 161−173.
(44) Sarkar, N. Thermal Gelation Properties of Methyl and Hydroxypropyl Methylcellulose. *J. Appl. Polym. Sci.* **1979**, *24*, 1073−1087.
(45) Nigmatullin, R.; Gabrielli, V.; Muñoz-García, J. C.; Lewandowska, A. E.; Harniman, R.; Khimyak, Y. Z.; Angulo, J.; Eichhorn, S. J. Thermosensitive Supramolecular and Colloidal Hydrogels via Self-Assembly Modulated by Hydrophobized Cellulose Nanocrystals. *Cellulose* **2019**, *26*, 529−542.
(46) Nasatto, P. L.; Pignon, F.; Silveira, J. L. M.; Duarte, M. E. R.; Noseda, M. D.; Rinaudo, M. Methylcellulose, a Cellulose Derivative with Original Physical Properties and Extended Applications. *Polymers* **2015**, *7*, 777−803.
(47) Chen, L.-H.; Cheng, L.-C.; Doyle, P.-S. Nanoemulsion-Loaded Capsules for Controlled Delivery of Lipophilic Active Ingredients. *Adv. Sci.* **2020**, 2001677.
(48) Gupta, A.; Eral, H. B.; Hatton, T. A.; Doyle, P. S. Nanoemulsions: Formation, Properties and Applications. *Soft Matter* **2016**, *12*, 2826−2841.
(49) Li, N.; Liu, E.; Lim, C. H. Micro-DSC and Rheological Studies of Interactions between Methylcellulose and Surfactants. *J. Phys. Chem. B* **2007**, *111*, 6410−6416.
(50) Gupta, A.; Eral, H. B.; Hatton, T. A.; Doyle, P. S. Controlling and Predicting Droplet Size of Nanoemulsions: Scaling Relations with Experimental Validation. *Soft Matter* **2016**, *12*, 1452−1458.
(51) Domenech, T.; Doyle, P. S. High Loading Capacity Nanoencapsulation and Release of Hydrophobic Drug Nanocrystals from Microgel Particles. *Chem. Mater.* **2020**, *32*, 498−509.
(52) Tipduangta, P.; Takieddin, K.; Fábián, L.; Belton, P.; Qi, S. A New Low Melting-Point Polymorph of Fenofibrate Prepared via Talc Induced Heterogeneous Nucleation. *Cryst. Growth Des.* **2015**, *15*, 5011−5020.
(53) Chen, L.-H.; Doyle, P. S. Design and Use of a Thermogelling Methylcellulose Nanoemulsion to Formulate Nanocrystalline Oral Dosage Forms. *Adv. Mater.* **2021**, *33*, 2008618.
(54) Jackson, C. L.; McKenna, G. B. The Melting Behavior of Organic Materials Confined in Porous Solids. *J. Chem. Phys.* **1990**, *93*, 9002−9011.
(55) Dwyer, L. M.; Michaelis, V. K.; O'Mahony, M.; Griffin, R. G.; Myerson, A. S. Confined Crystallization of Fenofibrate in Nanoporous Silica. *CrystEngComm* **2015**, *17*, 7922−7929.
(56) Godfrin, P. D.; Lee, H.; Lee, J. H.; Doyle, P. S. Photopolymerized Micelle-Laden Hydrogels Can Simultaneously Form and Encapsulate Nanocrystals to Improve Drug Substance Solubility and Expedite Drug Product Design. *Small* **2019**, *15*, 1803372.
(57) Heinz, A.; Gordon, K. C.; McGoverin, C. M.; Rades, T.; Strachan, C. J. Understanding the Solid-State Forms of Fenofibrate - A Spectroscopic and Computational Study. *Eur. J. Pharm. Biopharm.* **2009**, *71*, 100−108.
(58) Lee, M. K.; Jeon, T. Y.; Mun, C. W.; Kwon, J. D.; Yun, J.; Kim, S. H.; Kim, D. H.; Chang, S. C.; Park, S. G. 3D Multilayered Plasmonic Nanostructures with High Areal Density for SERS. *RSC Adv.* **2017**, *7*, 17898−17905.
(59) Jeon, T. Y.; Park, S. G.; Kim, D. H.; Kim, S. H. Standing-Wave-Assisted Creation of Nanopillar Arrays with Vertically Integrated Nanogaps for SERS-Active Substrates. *Adv. Funct. Mater.* **2015**, *25*, 4681−4688.
(60) Chen, H. Y.; Lin, M. H.; Wang, C. Y.; Chang, Y. M.; Gwo, S. Large-Scale Hot Spot Engineering for Quantitative SERS at the Single-Molecule Scale. *J. Am. Chem. Soc.* **2015**, *137*, 13698−13705.
(61) Eksi-Kocak, H.; Ilbasmis Tamer, S.; Yilmaz, S.; Eryilmaz, M.; Boyaci, I. H.; Tamer, U. Quantification and Spatial Distribution of Salicylic Acid in Film Tablets Using FT-Raman Mapping with Multivariate Curve Resolution. *Asian J. Pharm. Sci.* **2018**, *13*, 155−162.
(62) Kawabata, Y.; Wada, K.; Nakatani, M.; Yamada, S.; Onoue, S. Formulation Design for Poorly Water-Soluble Drugs Based on Biopharmaceutics Classification System: Basic Approaches and Practical Applications. *Int. J. Pharm.* **2011**, *420*, 1−10.
(63) *U.S. Food and Drug Administration − Dissolution Methods Database* https://www.accessdata.fda.gov/scripts/cder/dissolution/dsp_getalldata.cfm(accessed 2022-05-12)
(64) Zhou, Z.; Dunn, C.; Khadra, I.; Wilson, C. G.; Halbert, G. W. Influence of Physiological Gastrointestinal Surfactant Ratio on the Equilibrium Solubility of BCS Class II Drugs Investigated Using a Four Component Mixture Design. *Mol. Pharmaceutics* **2017**, *14*, 4132−4144.
(65) Amidon, G. L.; Lennernäs, H.; Shah, V. P.; Crison, J. R. A Theoretical Basis for a Biopharmaceutic Drug Classification: The Correlation of in Vitro Drug Product Dissolution and in Vivo Bioavailability. *Pharm. Res.* **1995**, *12*, 413−420.
(66) Jamzad, S.; Fassihi, R. Role of Surfactant and PH on Dissolution Properties of Fenofibrate and Glipizide - A Technical Note. *AAPS PharmSciTech* **2006**, *7*, E17−E22.

https://doi.org/10.1021/acs.chemmater.2c00801
Chem. Mater. XXXX, XXX, XXX−XXX

(67) Preis, M.; Woertz, C.; Schneider, K.; Kukawka, J.; Broscheit, J.; Roewer, N.; Breitkreutz, J. Design and Evaluation of Bilayered Buccal Film Preparations for Local Administration of Lidocaine Hydrochloride. *Eur. J. Pharm. Biopharm.* **2014**, *86*, 552−561.
(68) Reynolds, T. D.; Mitchell, S. A.; Balwinski, K. M. Investigation of the Effect of Tablet Surface Area/Volume on Drug Release from Hydroxypropylmethylcellulose Controlled-Release Matrix Tablets. *Drug Dev. Ind. Pharm.* **2002**, *28*, 457−466.
(69) Goyanes, A.; Robles Martinez, P.; Buanz, A.; Basit, A. W.; Gaisford, S. Effect of Geometry on Drug Release from 3D Printed Tablets. *Int. J. Pharm.* **2015**, *494*, 657−663.
(70) Van Eerdenbrugh, B.; Froyen, L.; Van Humbeeck, J.; Martens, J. A.; Augustijns, P.; Van den Mooter, G. Drying of Crystalline Drug Nanosuspensions-The Importance of Surface Hydrophobicity on Dissolution Behavior upon Redispersion. *Eur. J. Pharm. Sci.* **2008**, *35*, 127−135.
(71) Mou, D.; Chen, H.; Wan, J.; Xu, H.; Yang, X. Potent Dried Drug Nanosuspensions for Oral Bioavailability Enhancement of Poorly Soluble Drugs with PH-Dependent Solubility. *Int. J. Pharm.* **2011**, *413*, 237−244.
(72) Ritger, P. L.; Peppas, N. A. A Simple Equation for Description of Solute Release II. Fickian and Anomalous Release from Swellable Devices. *J. Controlled Release* **1987**, *5*, 37−42.
(73) Paarakh, M. P.; Jose, P. A.; Setty, C. M.; Peter, G. P. Release Kinetics − Concepts and Applications. *Int. J. Pharm. Res. Technol.* **2019**, *8*, 12−20.
(74) Hopfenberg, H. B. Controlled Release from Erodible Slabs, Cylinders, and Spheres. In *ACS Symposium Series*, 1976; Vol. *33*, pp. 26−32.
(75) Zhang, L.; Alfano, J.; Race, D.; Davé, R. N. Zero-Order Release of Poorly Water-Soluble Drug from Polymeric Films Made via Aqueous Slurry Casting. *Eur. J. Pharm. Sci.* **2018**, *117*, 245−254.
(76) Leon, R. A. L.; Wan, W. Y.; Badruddoza, A. Z. M.; Hatton, T. A.; Khan, S. A. Simultaneous Spherical Crystallization and Co-Formulation of Drug(s) and Excipient from Microfluidic Double Emulsions. *Cryst. Growth Des.* **2014**, *14*, 140−146.
(77) Llinàs, A.; Goodman, J. M. Polymorph Control: Past, Present and Future. *Drug Discovery Today* **2008**, *13*, 198−210.
(78) Leon, R. A. L.; Badruddoza, A. Z. M.; Zheng, L.; Yeap, E. W. Q.; Toldy, A. I.; Wong, K. Y.; Hatton, T. A.; Khan, S. A. Highly Selective, Kinetically Driven Polymorphic Selection in Microfluidic Emulsion-Based Crystallization and Formulation. *Cryst. Growth Des.* **2015**, *15*, 212−218.

https://doi.org/10.1021/acs.chemmater.2c00801
Chem. Mater. XXXX, XXX, XXX−XXX